Two routes from the Boltzmann equation to compressible flow of polyatomic gases

Paul J. Dellar
Department of Mathematics,
Imperial College London,
London SW7 2AZ,
United Kingdom
Email: paul.dellar@na-net.ornl.gov

Abstract: This paper presents a systematic approach to simulating compressible flow of polyatomic gases using the Boltzmann equation for a discrete set of particle velocities. We derive the complete system of moment equations needed to recover the Navier–Stokes–Fourier equations. One may either circumvent the usual relation between pressure and internal energy density by assigning additional energies to the particles, or introduce an entirely separate set of particle distribution functions to simulate the macroscopic energy equation. The latter permits the use of longer timesteps, and may generalise more easily to multiple space dimensions. However, the momentum and energy equations must be coupled to obtain correct viscous heating for realistic values of the Prandtl number. Numerical experiments are presented for the standard one dimensional Sod shock tube benchmark for monatomic and diatomic gases using both unified 7 velocity and split 4+3 velocity formulations.

Keywords: lattice Boltzmann; discrete kinetic theory; gas dynamics; shock waves; splitting methods

Reference to this paper should be made as follows: Dellar, P. J. (2008) 'Two routes from the Boltzmann equation to compressible flow of polyatomic gases', *Progress in Computational Fluid Dynamics* Vol. 8, Nos. 1/2/3/4 pp. 84–96.
DOI:10.1504/PCFD.2008.018081

Biographical notes: Paul Dellar graduated in mathematics from the University of Cambridge, and holds a PhD in applied mathematics from the same institution. At the time of writing he held a Lectureship in Applied Mathematics at Imperial College London, but he has since moved to the University of Oxford.

1 Introduction

The lattice Boltzmann method is now widely employed to simulate nearly incompressible fluid flows, most commonly using an isothermal equation. Efforts to simulate compressible flows with evolving temperatures at larger Mach numbers originally met with limited success, being far more susceptible to numerical instabilities [1, 5]. This led to a search for alternative equilibria offering improvements in numerical stability [26], but at the price of introducing unphysical artifacts such as spikes and compound waves into the solutions of the simulated equations [7].

However, it is now recognised that the lack of numerical stability is a consequence of the particular space/time discretisation employed in the lattice Boltzmann method, rather than any intrinsic defect in Boltzmann equation itself. The Boltzmann equation with a discrete velocity space, equation (1) below, is just a finite set of hyperbolic partial differential equations coupled by some algebraic source terms. Using alternative space/time discretisations designed for hyperbolic systems (for pioneering work see Refs. [22, 25]), it is possible to simulate standard benchmark problems such as the first Sod [20, 32] shock tube using a discrete velocity Boltzmann equation [9].

Before embarking on a study of Boltzmann-based methods for compressible flow, it is worth remarking that the

more established total variation diminishing (TVD) or Godunov-based methods (see *e.g.* Laney [20]) only attempt to recover entropy-satisfying solutions of the compressible Euler equations, without explicit treatment of non-ideal effects like viscosity and heat conduction. Moreover, these methods are known to malfunction in various scenarios due to a lack of sufficient dissipation, perhaps the most well-known being the spurious transonic rarefaction shocks computed by Roe's approximate Riemann solver [24, 27]. To take another example, a Godunov-based computation in magnetohydrodynamics showed incorrect behaviour due to an inaccurate treatment of dissipation in the magnetic field, as described in [8].

Xu's [39] gas kinetic BGK scheme offers an integrated treatment that combines the ideal Euler equations with viscosity and heat conduction. However, this approach reconstructs the distribution function as a truncated Chapman–Enskog expansion, with gradients of the velocity and temperature approximated using their values at grid points. In other words, the only degrees of freedom are the standard hydrodynamic variables of mass, momentum, and energy densities at grid points. A discrete or lattice Boltzmann approach provides independent evolution equations for the stress, heat flux, and higher moments of the distribution function. This may offer an improved approximation to continuum kinetic theory outside the small mean-free-path limit described by the Chapman–Enskog expansion, and motivates existing applications of the standard lattice Boltzmann method to rarefied flows of monatomic gases at small Mach numbers. These are currently confined to isothermal flows in relatively simple geometries, but a number of lattice Boltzmann implementations have been demonstrated that capture, at least qualitatively, second order slip flow and the so-called Knudsen minimum in microchannels [2, 35, 40]. However, a more satisfactory treatment would employ larger lattices in the discrete velocity space, chosen to reproduce the higher moments of the continuum Maxwell–Boltzmann distribution function that enter the derivation of the Burnett equations at second order in Knudsen number. The present paper is itself concerned with the adoption of larger lattices in discrete velocity space, but for the different purpose of simulating the correct energy equation for a polyatomic gas.

Turning to polyatomic gases, in any ideal gas the pressure p varies according to $p \propto \rho^\gamma$ under adiabatic changes in the density ρ. Kinetic theory gives the relation $\gamma = 1 + 2/D$ between the adiabatic exponent γ and the number D of degrees of freedom associated with molecule. This leads to the well-known $\gamma = 5/3$ for monatomic gases, each atom having 3 translational degrees of freedom. Much recent interest has been devoted to simulating the behaviour of gases in micro-electro-mechanical devices (MEMs). The gas is typically air, primarily a mixture of two diatomic gases nitrogen and oxygen. Diatomic molecules have 2 rotational degrees of freedom, rotation about the line of centres being forbidden quantum-mechanically, which combines with the 3 translational degrees of freedom to give $D = 5$ and $\gamma = 7/5$. The commercial heat transfer fluid known as PP10, the fluorocarbon $C_{13}F_{22}$, has $\gamma = 1.0128$ corresponding to $D \approx 39$. (Equality is not exact because the molecule comprises carbon and fluorine atoms with two different masses.)

Being based on the kinetic theory of monatomic gases, those with no internal degrees of freedom, the value for D in the standard lattice or discrete Boltzmann approach is just the number of spatial dimensions. Thus one obtains $D = 3$ and $\gamma = 5/3$ from a three dimensional computation, but $\gamma = 3$ in the purely one-dimensional formulation used in Ref. [9]. As it would be undesirable to formulate a lattice in 5, let alone 39, spatial dimensions merely to simulate flow of one of the above fluids, we shall investigate approaches that allow the adiabatic exponent γ to be varied independently of the number of spatial dimensions. Following earlier work on the classical kinetic theory of polyatomic gases [12, 23, 34], Shi *et al.* [30] and Kataoka and Tsutahara [14] equipped their particles with additional internal energies to circumvent the restrictions of the Boltzmann equation. However, Shi *et al.* [30] did not attempt to obtain correct viscous and conductive behaviour, being satisfied with the compressible Euler equations, while Kataoka and Tsutahara [14] postulate a form for their equilibrium distribution functions $f_i^{(0)}$ that typically leads to an unnecessarily large number of particle velocities.

Li *et al.* [21] developed a discrete Boltzmann approach for simulating aeroacoustics in diatomic gases. They retained the unmodified Boltzmann equation without internal energies, as presented in Sec. 2 below. Being concerned only with simulating small amplitude sound waves (acoustics) they adjusted the second moment of the equilibrium distribution to give the correct energy density for diatomic gases. The subsequently incorrect momentum flux tensor does not affect the propagation of sound waves, so this approach is perfectly sufficient for the purpose of simulating aeroacoustics. It is not, however, sufficient to simulate more general flows of diatomic gases. Li *et al.* [21] also implemented a temperature-dependent relaxation time that yields Sutherland's law for the temperature-dependent viscosity of a diatomic gas (see Sec. 10).

In this paper we give a systematic treatment, first deriving necessary and sufficient conditions to recover the Navier–Stokes–Fourier equations exactly, then investigating two alternative implementations. One may either use a single set of particle to reproduce the continuity, momentum, and energy equations, or introduce a second set of particles to reproduce only the energy equation. The latter may be more amenable to implementation in multiple space dimensions, but it is necessary to couple the two sets of particles through the collision operator to obtain the correct viscous heating when the Prandtl number is set to a realistic value.

Our approach is valid in the limit of a rapid equipartition of energy between the translational and rotational degrees of freedom, for which the gas may be described by the Navier–Stokes–Fourier equations with an arbitrary (but constant) adiabatic exponent γ. A more sophisti-

cated treatment with a separate evolution equation for the internal energy becomes necessary when the timescale for exchange of energy between translational and rotational degrees of freedom is comparable to hydrodynamic timescales. At the other extreme, when hydrodynamic timescales are short compared with the timescale for internal energy exchange, the internal degrees of freedom become "frozen" and the gas behaves as though it were monatomic (*e.g.* [16]). In addition, real gas molecules contain different kinds of internal degrees of freedom, or modes. For example, a diatomic molecule has a vibrational mode in addition to the rotational modes described above. The vibrational mode is typically frozen at room temperature, but may become excited at higher temperatures. This leads to an effective change in the adiabatic exponent γ with temperature, as each additional internal mode moves from being frozen, through evolving on a hydrodynamic timescale, to a rapid equipartition with the translational degrees of freedom. The approach in this paper is limited to constant γ.

2 Moments of the Boltzmann equation

The discrete Boltzmann equation is an evolution equation for a finite set of distribution functions $f_i(\mathbf{x}, t)$,

$$\partial_t f_i + \boldsymbol{\xi}_i \cdot \nabla f_i = -\frac{1}{\tau}\left(f_i - f_i^{(0)}\right). \tag{1}$$

Each f_i represents the number density of particles moving with velocity $\boldsymbol{\xi}_i$. On the right hand side we have written the Bhatnagar, Gross, Krook (BGK) collision operator [3], under which the f_i relax towards some explicitly specified equilibria $f_i^{(0)}$ with a single relaxation time τ. The choice of a BGK collision operator, and a fixed τ, is adopted for simplicity of presentation, and will be briefly revisited later. The common objection that the BGK collision operator yields suboptimal stability with the space/time discretisation of (1) used in the lattice Boltzmann method is not relevant for the alternative space/time discretisation that we describe in Sec. 9 below.

The macroscopic mass (ρ), momentum ($\rho\mathbf{u}$), and energy ($\mathcal{E}$) densities are typically defined by moments of the distribution functions,

$$\rho = \sum_{i=0}^{N} f_i, \quad \rho\mathbf{u} = \sum_{i=0}^{N} \boldsymbol{\xi}_i f_i, \quad \mathcal{E} = \frac{1}{2}\sum_{i=0}^{N} |\boldsymbol{\xi}_i|^2 f_i, \tag{2}$$

where $\mathbf{u}$ is the fluid velocity. The equilibria $f_i^{(0)}$ are then constructed as functions of these macroscopic quantities in such a way that

$$\sum_{i=0}^{N} f_i^{(0)} = \rho, \quad \sum_{i=0}^{N} \boldsymbol{\xi}_i f_i^{(0)} = \rho\mathbf{u}, \quad \frac{1}{2}\sum_{i=0}^{N} |\boldsymbol{\xi}_i|^2 f_i^{(0)} = \mathcal{E}. \tag{3}$$

To clarify, the former equations (2) are *definitions* of the quantities ρ, $\mathbf{u}$, and $\mathcal{E}$, while the latter equations (3) are *constraints* on the functional form of the $f_i^{(0)}$ expressed in terms of the quantities ρ, $\mathbf{u}$, and $\mathcal{E}$. These constraints ensure that mass, momentum, and energy are conserved under the BGK model of collisions, just as they are conserved by Boltzmann's original binary collision operator. Requiring the existence of a solution $f_i^{(0)}$ to these constraints, and of the further constraints derived below, in turn imposes constraints on the $\boldsymbol{\xi}_i$ in a more subtle manner.

From moments of the Boltzmann equation (1) we obtain exact conservation laws for the macroscopic mass, momentum, and energy densities,

$$\partial_t \rho + \nabla\cdot(\rho\mathbf{u}) = 0, \quad \partial_t(\rho\mathbf{u}) + \nabla\cdot\boldsymbol{\Pi} = 0, \quad \partial_t \mathcal{E} + \nabla\cdot\boldsymbol{\mathcal{F}} = 0. \tag{4}$$

The right hand sides vanish due to equations (3). The momentum flux (or stress) tensor $\boldsymbol{\Pi}$ and the energy flux vector $\boldsymbol{\mathcal{F}}$ are identified as higher moments of the distribution functions,

$$\boldsymbol{\Pi} = \sum_{i=0}^{N} \boldsymbol{\xi}_i\boldsymbol{\xi}_i f_i, \quad \boldsymbol{\mathcal{F}} = \frac{1}{2}\sum_{i=0}^{N} |\boldsymbol{\xi}_i|^2 \boldsymbol{\xi}_i f_i. \tag{5}$$

The compressible Euler equations follow from (4) when $\boldsymbol{\Pi}$ and $\boldsymbol{\mathcal{F}}$ are approximated by their equilibrium values, which must be

$$\boldsymbol{\Pi}^{(0)} = \sum_{i=0}^{N} \boldsymbol{\xi}_i\boldsymbol{\xi}_i f_i^{(0)} = p\mathsf{I} + \rho\mathbf{u}\mathbf{u}, \tag{6}$$

$$\boldsymbol{\mathcal{F}}^{(0)} = \frac{1}{2}\sum_{i=0}^{N} |\boldsymbol{\xi}_i|^2 \boldsymbol{\xi}_i f_i^{(0)} = \mathbf{u}(\mathcal{E} + p), \tag{7}$$

where p is the fluid pressure. These equations should thus be interpreted as imposing additional constraints on the equilibria $f_i^{(0)}$. An expression for the pressure p in terms of the conserved quantities ρ, $\mathbf{u}$, $\mathcal{E}$ will be given in the following section.

The Navier–Stokes–Fourier equations follow by formulating evolution equations for the higher moments, for instance

$$\partial_t \boldsymbol{\Pi} + \nabla\cdot\left(\sum_{i=0}^{N} \boldsymbol{\xi}_i\boldsymbol{\xi}_i\boldsymbol{\xi}_i f_i\right) = -\frac{1}{\tau}\left(\boldsymbol{\Pi} - \boldsymbol{\Pi}^{(0)}\right), \tag{8}$$

and using a Chapman–Enskog expansion to seek solutions that vary slowly compared with the collisional timescale τ. This is equivalent to expanding the momentum and energy fluxes as series in a small parameter ϵ,

$$\boldsymbol{\Pi} = \boldsymbol{\Pi}^{(0)} + \epsilon\boldsymbol{\Pi}^{(1)} + \cdots, \quad \boldsymbol{\mathcal{F}} = \boldsymbol{\mathcal{F}}^{(0)} + \epsilon\boldsymbol{\mathcal{F}}^{(1)} + \cdots, \tag{9}$$

where ϵ is the ratio of τ to a characteristic hydrodynamic timescale. The conserved quantities ρ, $\mathbf{u}$, and $\mathcal{E}$ are left unexpanded, since they do not evolve on a collisional timescale. One then uses the corresponding multiple-scales expansion of the time derivative

$$\partial_t = \partial_{t_0} + \epsilon\partial_{t_1} + \cdots \tag{10}$$

to justify replacing ∂_t by ∂_{t_0} in equation (8) and its analogue for $\boldsymbol{\mathcal{F}}$. Further details are presented in Sec. 4 for the momentum flux, and Sec. 5 for the energy flux.

3 Introduction of internal energies

Comparing equations (3) and (7), we see that there is a relation between the energy density $\mathcal{E}$ and the trace of the equilibrium momentum flux tensor $\mathbf{\Pi}^{(0)}$,

$$\mathcal{E} = \frac{1}{2}\sum_{i=0}^{N} |\boldsymbol{\xi}_i|^2 f_i^{(0)} = \frac{1}{2}\mathrm{Tr}\sum_{i=0}^{N} \boldsymbol{\xi}_i\boldsymbol{\xi}_i f_i^{(0)} = \frac{1}{2}\mathrm{Tr}\,\mathbf{\Pi}^{(0)}. \quad (11)$$

Substituting $\Pi^{(0)} = p\mathsf{I} + \rho\mathbf{uu}$ as given by the compressible Euler equations, we obtain

$$\mathcal{E} = \frac{D}{2}p + \frac{1}{2}\rho|\mathbf{u}|^2, \quad (12)$$

where the number of spatial dimensions D enters through $\mathrm{Tr}\,\mathsf{I} = D$. Comparing equation (12) with the standard expression for an ideal gas [19]

$$\mathcal{E} = \frac{p}{\gamma-1} + \frac{1}{2}\rho|\mathbf{u}|^2, \quad (13)$$

establishes the relation $\gamma = 1+2/D$ between D and the adiabatic exponent γ.

Following earlier work on the classical kinetic theory of polyatomic gases [12, 23, 34], Shi *et al.* [30] and Kataoka and Tsutahara [14] circumvented this restriction on γ by postulating an additional internal energy ϵ_i for each particle, in addition to the particle's kinetic energy proportional to $|\boldsymbol{\xi}_i|^2$. They thus replaced the previous definitions of the macroscopic energy density and energy flux by

$$\mathcal{E} = \frac{1}{2}\sum_{i=0}^{N}\left(|\boldsymbol{\xi}_i|^2+\epsilon_i\right) f_i, \quad \boldsymbol{\mathcal{F}} = \frac{1}{2}\sum_{i=0}^{N}\left(|\boldsymbol{\xi}_i|^2+\epsilon_i\right)\boldsymbol{\xi}_i f_i. \quad (14)$$

Having postulated the expression for $\mathcal{E}$, the expression for $\boldsymbol{\mathcal{F}}$ follows from comparing the desired energy equation

$$\partial_t\mathcal{E} + \nabla\cdot\boldsymbol{\mathcal{F}} = 0 \quad (15)$$

with the Boltzmann equation (1). Note that the ϵ_i must be prescribed constants, so that they may be taken inside spatial and temporal derivatives to construct evolution equations for the moments.

To obtain the compressible Euler equations at leading order, we require [19]

$$\mathcal{E}^{(0)} = \frac{1}{2}\sum_{i=0}^{N}\left(|\boldsymbol{\xi}_i|^2+\epsilon_i\right) f_i^{(0)} = \frac{p}{\gamma-1} + \frac{1}{2}\rho|\mathbf{u}|^2, \quad (16)$$

$$\boldsymbol{\mathcal{F}}^{(0)} = \frac{1}{2}\sum_{i=0}^{N}\left(|\boldsymbol{\xi}_i|^2+\epsilon_i\right)\boldsymbol{\xi}_i f_i^{(0)} = \frac{\gamma}{\gamma-1}p\mathbf{u} + \frac{1}{2}\rho|\mathbf{u}|^2\mathbf{u}. \quad (17)$$

These equations should be interpreted as constraints on both the $f_i^{(0)}$ and the internal energies ϵ_i.

For future convenience, and following standard terminology in the lattice Boltzmann literature, we introduce a temperature θ such that $p = \theta\rho$. This temperature is measured in so-called energy units that absorb Boltzmann's constant, or the molar gas constant R. The temperature is then equal to the square of the isothermal or Newtonian sound speed, $c_\mathrm{s} = (p/\rho)^{1/2} = \theta^{1/2}$.

An alternative definition of temperature for a polyatomic gas uses only the translational degrees of freedom [16]. This alternative definition leads to a $\nabla\cdot\mathbf{u}$ term in the relation between pressure and temperature, in place of the bulk viscous stress proportional to $\nabla\cdot\mathbf{u}$ that we calculate below. For example, Kogan's [15] treatment using the translational temperature yields exactly the same expression $-\tau\rho\theta(5/3-\gamma)\nabla\cdot\mathbf{u}$ that we give in (23) below, but as a non-equilibrium contribution to the pressure rather than an isotropic contribution to the viscous stress from bulk viscosity.

4 Calculation of the viscous stress

Following the standard Chapman–Enskog approach, we obtain an explicit formula for the viscous stress from the evolution equation (8) by evaluating the left hand side using the equilibrium distributions $f_i^{(0)}$, and approximating the time derivative using the compressible Euler equations,

$$\partial_{t_0}\mathbf{\Pi}^{(0)} + \nabla\cdot\left(\sum_{i=0}^{N}\boldsymbol{\xi}_i\boldsymbol{\xi}_i\boldsymbol{\xi}_i f_i^{(0)}\right) = -\frac{1}{\tau}\mathbf{\Pi}^{(1)}. \quad (18)$$

The first term $\partial_{t_0}\mathbf{\Pi}^{(0)} = \partial_{t_0}\left(\rho\mathbf{uu} + \rho\theta\mathsf{I}\right)$ evaluates to

$$\begin{aligned}
\partial_{t_0}\mathbf{\Pi}^{(0)} &= \partial_{t_0}(\rho\mathbf{u})\mathbf{u} + \mathbf{u}\partial_{t_0}(\rho\mathbf{u}) - \mathbf{uu}\partial_{t_0}\rho + \partial_{t_0}(\rho\theta)\mathsf{I}, \\
&= -\nabla\cdot(\rho\mathbf{uu} + \rho\theta\mathsf{I})\mathbf{u} - \mathbf{u}\nabla\cdot(\rho\mathbf{uu} + \rho\theta\mathsf{I}) \\
&\quad + \mathbf{uu}\nabla\cdot(\rho\mathbf{u}) - \nabla\cdot(\rho\theta\mathbf{u})\mathsf{I} - (\gamma-1)(\rho\theta\nabla\cdot\mathbf{u})\mathsf{I}, \\
&= -\nabla\cdot(\rho\mathbf{uuu}) - \nabla(\rho\theta)\mathbf{u} - \mathbf{u}\nabla(\rho\theta) \\
&\quad -\nabla\cdot(\rho\theta\mathbf{u})\mathsf{I} - (\gamma-1)(\rho\theta\nabla\cdot\mathbf{u})\mathsf{I}, \quad (19)
\end{aligned}$$

after using the Euler momentum and temperature equations in the form

$$\begin{aligned}
\partial_{t_0}(\rho\mathbf{u}) &+ \nabla\cdot(\rho\mathbf{uu} + \rho\theta\mathsf{I}) = 0, \\
\partial_{t_0}(\rho\theta) &+ \nabla\cdot(\rho\theta\mathbf{u}) + (\gamma-1)\rho\theta\nabla\cdot\mathbf{u} = 0. \quad (20)
\end{aligned}$$

To cancel the $\rho\mathbf{uuu}$ and $\nabla(\rho\theta)$ terms in (19) we must choose the equilibrium distribution $f_i^{(0)}$ to satisfy

$$\sum_{i=0}^{N}\boldsymbol{\xi}_i\boldsymbol{\xi}_i\boldsymbol{\xi}_i f_i^{(0)} = \rho\mathbf{uuu} + \rho\theta\left(\mathbf{u}\,\mathsf{I} + \mathrm{cyclic}\right). \quad (21)$$

The expression $(\mathbf{u}\,\mathsf{I} + \mathrm{cyclic})$ denotes the completely symmetric third rank tensor with components $u_\alpha\delta_{\beta\gamma} + u_\beta\delta_{\gamma\alpha} + u_\gamma\delta_{\alpha\beta}$ that cannot be written in dyadic notation. Substituting (19) and (21) into (18), we obtain

$$\Pi^{(1)}_{\alpha\beta} = -\tau\rho\theta\left(\frac{\partial u_\alpha}{\partial x_\beta} + \frac{\partial u_\beta}{\partial x_\alpha} - (\gamma-1)\delta_{\alpha\beta}\frac{\partial u_\gamma}{\partial x_\gamma}\right), \quad (22)$$

which is a Newtonian viscous stress with shear viscosity $\mu = \tau\rho\theta$. It may be rewritten in a more illuminating form as

$$\boldsymbol{\Pi}^{(1)} = -\tau\rho\theta\left[(\nabla\mathbf{u}) + (\nabla\mathbf{u})^{\mathsf{T}} - \frac{2}{3}\mathsf{I}\nabla\cdot\mathbf{u}\right] - \tau\rho\theta\left(\frac{5}{3} - \gamma\right)\mathsf{I}\nabla\cdot\mathbf{u}. \tag{23}$$

The first term, having zero trace, is the standard viscous stress for a dilute monatomic gas (for which $\gamma = 5/3$) obtained from classical kinetic theory. The second term is an additional bulk viscous stress with bulk viscosity $(5/3-\gamma)\mu$ that arises from changing the adiabatic exponent γ. This definition of bulk viscosity is always positive when $\gamma < 5/3$, corresponding to *additional* internal degrees of freedom ($D > 3$ in $\gamma = 1+2/D$), but different authors use different conventions for what constitutes "bulk viscosity". Some authors use this phrase for the whole of the isotropic term in (22), rather than just that part adding to the traceless first term in (23), as listed in [6].

In summary, the constraints (3), (7), and (21) on the equilibrium distribution functions $f_i^{(0)}$ are necessary and sufficient to yield the continuity and momentum equations with a Newtonian viscous stress as above. The only use we have made of the energy equation is through eliminating $\partial_{t_0}(\rho\theta)$ using the compressible Euler temperature equation to derive (19).

5 Calculation of heat conduction and viscous heating

Similarly, we calculate the corrections to the energy flux $\boldsymbol{\mathcal{F}}^{(0)}$ that are responsible for heat conduction and viscous heating by first formulating an evolution equation for $\boldsymbol{\mathcal{F}}$. Taking the $\frac{1}{2}(|\boldsymbol{\xi}_i|^2+\epsilon_i)\boldsymbol{\xi}_i$ moment of the Boltzmann equation gives

$$\partial_t\boldsymbol{\mathcal{F}} + \nabla\cdot\left(\frac{1}{2}\sum_{i=0}^{N}(|\boldsymbol{\xi}_i|^2+\epsilon_i)\,\boldsymbol{\xi}_i\boldsymbol{\xi}_i f_i\right) = -\frac{1}{\tau}\left(\boldsymbol{\mathcal{F}} - \boldsymbol{\mathcal{F}}^{(0)}\right), \tag{24}$$

which, to sufficient accuracy, again simplifies to

$$\partial_{t_0}\boldsymbol{\mathcal{F}}^{(0)} + \nabla\cdot\left(\frac{1}{2}\sum_{i=0}^{N}(|\boldsymbol{\xi}_i|^2+\epsilon_i)\,\boldsymbol{\xi}_i\boldsymbol{\xi}_i f_i^{(0)}\right) = -\frac{1}{\tau}\boldsymbol{\mathcal{F}}^{(1)} \tag{25}$$

when using the Chapman–Enskog expansion. Evaluating $\partial_{t_0}\boldsymbol{\mathcal{F}}^{(0)}$ step by step, we find

$$\begin{aligned}
\partial_{t_0}(\rho\theta\mathbf{u}) &= \mathbf{u}\partial_{t_0}(\rho\theta) + \theta\partial_{t_0}(\rho\mathbf{u}) - \mathbf{u}\theta\partial_{t_0}\rho,\\
&= -\mathbf{u}\left[\nabla\cdot(\rho\mathbf{u}\theta) + (\gamma-1)\rho\theta\nabla\cdot\mathbf{u}\right]\\
&\quad -\theta\nabla\cdot(\rho\mathbf{u}\mathbf{u} + \rho\theta\mathsf{I}) + \mathbf{u}\theta\nabla\cdot(\rho\mathbf{u}),\\
&= -(\gamma-1)\rho\theta\mathbf{u}\nabla\cdot\mathbf{u} - \theta\nabla(\rho\theta) - \nabla\cdot(\rho\theta\mathbf{u}\mathbf{u}),
\end{aligned} \tag{26}$$

and

$$\begin{aligned}
&\partial_{t_0}\left(\tfrac{1}{2}\,\rho\mathbf{u}|\mathbf{u}|^2\right)\\
&\quad= \frac{1}{2}|\mathbf{u}|^2\partial_{t_0}(\rho\mathbf{u}) + \mathbf{u}\,\mathbf{u}\cdot\partial_{t_0}(\rho\mathbf{u}) - \mathbf{u}|\mathbf{u}|^2\partial_{t_0}\rho,\\
&\quad= -\frac{1}{2}|\mathbf{u}|^2\nabla\cdot(\rho\mathbf{u}\mathbf{u} + \rho\theta\mathsf{I}),\\
&\qquad -\mathbf{u}\,\mathbf{u}\cdot\nabla\cdot(\rho\mathbf{u}\mathbf{u} + \rho\theta\mathsf{I}) + \mathbf{u}|\mathbf{u}|^2\nabla\cdot(\rho\mathbf{u}),\\
&\quad= -\frac{1}{2}\nabla\cdot(\rho\mathbf{u}\mathbf{u}|\mathbf{u}|^2) - \frac{1}{2}|\mathbf{u}|^2\nabla(\rho\theta) - \mathbf{u}\mathbf{u}\cdot\nabla(\rho\theta),\\
&\quad= -\nabla\cdot\left[\frac{1}{2}\rho\mathbf{u}\mathbf{u}|\mathbf{u}|^2 + \frac{1}{2}|\mathbf{u}|^2\rho\theta\mathsf{I} + \rho\theta\mathbf{u}\mathbf{u}\right],\\
&\qquad +\rho\theta\nabla\frac{1}{2}|\mathbf{u}|^2 + \rho\theta\nabla\cdot(\mathbf{u}\mathbf{u}).
\end{aligned} \tag{27}$$

Assembling the two halves,

$$\begin{aligned}
&\partial_{t_0}\,\boldsymbol{\mathcal{F}}^{(0)}\\
&= \partial_{t_0}\left(\frac{1}{2}\rho\mathbf{u}|\mathbf{u}|^2 + \frac{\gamma}{\gamma-1}\rho\theta\mathbf{u}\right)\\
&= \nabla\cdot\left[\frac{1}{2}\rho\mathbf{u}\mathbf{u}|\mathbf{u}|^2 + \frac{1}{2}|\mathbf{u}|^2\rho\theta\mathsf{I} + \frac{2\gamma-1}{\gamma-1}\rho\theta\mathbf{u}\mathbf{u} + \frac{\gamma}{\gamma-1}\rho\theta^2\mathsf{I}\right]\\
&\quad +\rho\theta\left[u_\alpha\nabla u_\alpha + \mathbf{u}\cdot\nabla\mathbf{u} - (\gamma-1)\mathbf{u}\nabla\cdot\mathbf{u}\right] + \frac{\gamma}{\gamma-1}\rho\theta\nabla\theta,\\
&= \nabla\cdot\left[\frac{1}{2}\rho\mathbf{u}\mathbf{u}|\mathbf{u}|^2 + \frac{1}{2}|\mathbf{u}|^2\rho\theta\mathsf{I} + \frac{2\gamma-1}{\gamma-1}\rho\theta\mathbf{u}\mathbf{u} + \frac{\gamma}{\gamma-1}\rho\theta^2\mathsf{I}\right]\\
&\quad -\frac{1}{\tau}\mathbf{u}\cdot\boldsymbol{\Pi}^{(1)} + \frac{\gamma}{\gamma-1}\rho\theta\nabla\theta.
\end{aligned} \tag{28}$$

Choosing the $f_i^{(0)}$ so that the term whose divergence appears in (25) cancels the divergence term $\nabla\cdot[\ ]$ in (28),

$$\frac{1}{2}\sum_{i=0}^{N}\left(|\boldsymbol{\xi}_i|^2+\epsilon_i\right)\boldsymbol{\xi}_i\boldsymbol{\xi}_i f_i^{(0)} = \frac{1}{2}\rho|\mathbf{u}|^2\mathbf{u}\mathbf{u} + \frac{1}{2}\rho\theta|\mathbf{u}|^2\mathsf{I} + \frac{2\gamma-1}{\gamma-1}\rho\theta\mathbf{u}\mathbf{u} + \frac{\gamma}{\gamma-1}\rho\theta^2\mathsf{I}, \tag{29}$$

therefore gives the desired viscous heating and conductive heat flux,

$$\boldsymbol{\mathcal{F}}^{(1)} = \mathbf{u}\cdot\boldsymbol{\Pi}^{(1)} - \frac{\gamma}{\gamma-1}\tau\rho\theta\nabla\theta. \tag{30}$$

The first term is the rate of working by viscous stresses, while the second term gives Fourier's law with thermal conductivity $\kappa = \tau\rho\theta\gamma/(\gamma-1)$.

Given that the right hand side of (29) must be a second rank symmetric tensor with the dimensions of $\rho|\mathbf{u}|^4$, a reasonable alternative to the above calculation is to postulate the functional form of (29) with four arbitrary constants in place of $1/2$, $\gamma/(\gamma-1)$, etc. Evaluating the left hand side of (25) using a symbolic manipulator package, the four constants may be adjusted to eliminate any appearance of $\nabla\rho$ in the heat flux. This procedure yields the unique coefficients given in (29).

6 Constraints on the equilibria and internal energies

To summarise, the equations of mass and momentum conservation with a Newtonian viscous stress determine the moments

$$\begin{aligned}\sum_{i=0}^{N} f_i^{(0)} &= \rho, \quad \sum_{i=0}^{N} \boldsymbol{\xi}_i f_i^{(0)} = \rho \mathbf{u}, \\ \boldsymbol{\Pi}^{(0)} &= \sum_{i=0}^{N} \boldsymbol{\xi}_i \boldsymbol{\xi}_i f_i^{(0)} = \rho\theta \mathsf{I} + \rho \mathbf{u}\mathbf{u}, \quad (31) \\ \sum_{i=0}^{N} \boldsymbol{\xi}_i \boldsymbol{\xi}_i \boldsymbol{\xi}_i f_i^{(0)} &= \rho \mathbf{u}\mathbf{u}\mathbf{u} + \rho\theta \left(\mathbf{u}\,\mathsf{I} + \text{cyclic}\right).\end{aligned}$$

The compressible Euler energy equation determines

$$\begin{aligned}\frac{1}{2}\sum_{i=0}^{N} \left(|\boldsymbol{\xi}_i|^2 + \epsilon_i\right) f_i^{(0)} &= \frac{\rho\,\theta}{\gamma - 1} + \frac{1}{2}\rho|\mathbf{u}|^2, \quad (32) \\ \frac{1}{2}\sum_{i=0}^{N} \left(|\boldsymbol{\xi}_i|^2 + \epsilon_i\right) \boldsymbol{\xi}_i f_i^{(0)} &= \frac{\gamma}{\gamma - 1}\rho\,\theta\,\mathbf{u} + \frac{1}{2}\rho|\mathbf{u}|^2\mathbf{u},\end{aligned}$$

and the conductive heat flux and viscous heating together determine

$$\begin{aligned}\frac{1}{2}\sum_{i=0}^{N} \left(|\boldsymbol{\xi}_i|^2 + \epsilon_i\right) \boldsymbol{\xi}_i \boldsymbol{\xi}_i f_i^{(0)} &= \frac{1}{2}\rho|\mathbf{u}|^2\mathbf{u}\mathbf{u} + \frac{1}{2}\rho\theta|\mathbf{u}|^2\mathsf{I} \quad (33) \\ &\quad + \frac{2\gamma - 1}{\gamma - 1}\rho\theta\mathbf{u}\mathbf{u} + \frac{\gamma}{\gamma - 1}\rho\theta^2\mathsf{I}.\end{aligned}$$

By contracting equations (31) on two indices, we find that the ϵ_i-independent contributions to (32) are already determined to be

$$\begin{aligned}\frac{1}{2}\sum_{i=0}^{N} |\boldsymbol{\xi}_i|^2 f_i^{(0)} &= \frac{D}{2}\rho\theta + \frac{1}{2}\rho|\mathbf{u}|^2, \\ \frac{1}{2}\sum_{i=0}^{N} |\boldsymbol{\xi}_i|^2 \boldsymbol{\xi}_i f_i^{(0)} &= \frac{1}{2}\rho|\mathbf{u}|^2\mathbf{u} + \frac{2 + D}{2}\rho\theta\mathbf{u}, \quad (34)\end{aligned}$$

so to satisfy equations (32) in addition we need

$$\begin{aligned}\frac{1}{2}\sum_{i=0}^{N} \epsilon_i f_i^{(0)} &= \left(\frac{1}{\gamma - 1} - \frac{D}{2}\right)\rho\theta, \\ \frac{1}{2}\sum_{i=0}^{N} \epsilon_i \boldsymbol{\xi}_i f_i^{(0)} &= \left(\frac{1}{\gamma - 1} - \frac{D}{2}\right)\rho\theta\mathbf{u}, \quad (35)\end{aligned}$$

where D is the number of spatial dimensions as before.

Since the fourth moment does not enter the momentum equation at viscous order, there is no unique way to split (33) between the $|\boldsymbol{\xi}_i|^2$ and ϵ_i contributions. However, it might seem reasonable to adopt the $\gamma = 5/3$ value for the $|\boldsymbol{\xi}_i|^2$ contribution, so that the ϵ_i are responsible for all deviations from monatomic gas behaviour. This gives

$$\frac{1}{2}\sum_{i=0}^{N} |\boldsymbol{\xi}_i|^2 \boldsymbol{\xi}_i \boldsymbol{\xi}_i f_i^{(0)} = \frac{1}{2}\rho|\mathbf{u}|^2\mathbf{u}\mathbf{u} + \frac{1}{2}\rho\theta|\mathbf{u}|^2\mathsf{I} + \frac{7}{2}\rho\theta\mathbf{u}\mathbf{u} + \frac{5}{2}\rho\theta^2\mathsf{I}, \quad (36)$$

where we note that the two $O(|\mathbf{u}|^2)$ terms arise from the contraction on two indices of the completely symmetric fourth rank tensor with components $u_\alpha u_\beta \delta_{\gamma\delta} + \cdots$ as required by the structure of the left hand side.

The γ-dependent contribution that remains for the ϵ_i terms is then

$$\frac{1}{2}\sum_{i=0}^{N} |\boldsymbol{\xi}_i|^2 \epsilon_i f_i^{(0)} = \left(\frac{1}{\gamma - 1} - \frac{D}{2}\right)\left(\rho\theta\mathbf{u}\mathbf{u} + \rho\theta^2\mathsf{I}\right), \quad (37)$$

which establishes the pattern of relations

$$\begin{aligned}\frac{1}{2}\sum_{i=0}^{N} \epsilon_i f_i^{(0)} &= \left(\frac{1}{\gamma - 1} - \frac{D}{2}\right)\theta\sum_{i=0}^{N} f_i^{(0)}, \\ \frac{1}{2}\sum_{i=0}^{N} \epsilon_i \boldsymbol{\xi}_i f_i^{(0)} &= \left(\frac{1}{\gamma - 1} - \frac{D}{2}\right)\theta\sum_{i=0}^{N} \boldsymbol{\xi}_i f_i^{(0)}, \quad (38) \\ \frac{1}{2}\sum_{i=0}^{N} \epsilon_i \boldsymbol{\xi}_i \boldsymbol{\xi}_i f_i^{(0)} &= \left(\frac{1}{\gamma - 1} - \frac{D}{2}\right)\theta\sum_{i=0}^{N} \boldsymbol{\xi}_i \boldsymbol{\xi}_i f_i^{(0)},\end{aligned}$$

between the ϵ_i moments and the lower moments appearing in the continuity and momentum equations. Unfortunately, taking the ϵ_i proportional to θ as suggested by this pattern is not possible. The ϵ_i must be constants, so that they commute with spatial and temporal derivatives, to obtain moment equations in conservation form as above.

7 One dimensional, unsplit seven velocity model

Each constraint equation has only one component in one spatial dimension. There are thus four constraints (31) from the momentum equation, and another three, (32) and (33), from the energy equation. This suggests choosing seven velocities with $\xi_i = i$ for $i = -3, \ldots, 3$. The ϵ_i must be chosen so that $\{\epsilon_i, \xi_i\epsilon_i, \xi_i^2\epsilon_i\}$ and $\{1, \xi_i, \xi_i^2, \xi_i^3\}$ comprise seven linearly independent vectors in $\mathbb{R}^7$. These vectors are the rows of the 7×7 matrix appearing below. One such choice is $\epsilon_i = (0, 0, 1, 4, 1, 0, 0)$, motivated by the three-velocity isothermal lattice Boltzmann equilibria. The perhaps more natural rescaling $\epsilon_i = (0, 0, 1/6, 2/3, 1/6, 0, 0)$ leads to a far less stable numerical scheme.

Given the ϵ_i, the constraints (31) to (33) may be written

as a system of seven linear equations for the seven $f_i^{(0)}$,

$$\begin{pmatrix} 1 & 1 & 1 & 1 & 1 & 1 & 1 \\ -3 & -2 & -1 & 0 & 1 & 2 & 3 \\ 9 & 4 & 1 & 0 & 1 & 4 & 9 \\ -27 & -8 & -1 & 0 & 1 & 8 & 27 \\ 9 & 4 & 2 & 4 & 2 & 4 & 9 \\ -27 & -8 & -2 & 0 & 2 & 8 & 27 \\ 81 & 16 & 2 & 0 & 2 & 16 & 81 \end{pmatrix} \begin{pmatrix} f_{-3}^{(0)} \\ f_{-2}^{(0)} \\ f_{-1}^{(0)} \\ f_0^{(0)} \\ f_1^{(0)} \\ f_2^{(0)} \\ f_3^{(0)} \end{pmatrix}$$

$$= \rho \begin{pmatrix} 1 \\ u \\ u^2+\theta \\ u^3+3\theta u \\ u^2+2\theta/(\gamma-1) \\ u^3+2\theta u\,\gamma/(\gamma-1) \\ u^4+\theta u^2(5\gamma-3)/(\gamma-1)+2\theta^2\gamma/(\gamma-1) \end{pmatrix}. \quad (39)$$

Subtracting the third row from the fifth row, and the fourth row from the sixth row, leads to some simplification,

$$\begin{pmatrix} 1 & 1 & 1 & 1 & 1 & 1 & 1 \\ -3 & -2 & -1 & 0 & 1 & 2 & 3 \\ 9 & 4 & 1 & 0 & 1 & 4 & 9 \\ -27 & -8 & -1 & 0 & 1 & 8 & 27 \\ 0 & 0 & 1 & 4 & 1 & 0 & 0 \\ 0 & 0 & -1 & 0 & 1 & 0 & 0 \\ 81 & 16 & 2 & 0 & 2 & 16 & 81 \end{pmatrix} \begin{pmatrix} f_{-3}^{(0)} \\ f_{-2}^{(0)} \\ f_{-1}^{(0)} \\ f_0^{(0)} \\ f_1^{(0)} \\ f_2^{(0)} \\ f_3^{(0)} \end{pmatrix}$$

$$= \rho \begin{pmatrix} 1 \\ u \\ u^2+\theta \\ u^3+3\theta u \\ \theta(\gamma-3)/(\gamma-1) \\ \theta u(\gamma-3)/(\gamma-1) \\ u^4+\theta u^2(5\gamma-3)/(\gamma-1)+2\theta^2\gamma/(\gamma-1) \end{pmatrix}. \quad (40)$$

Having chosen the ϵ_i to ensure linear independence of the rows of the matrices in (39) and (40), either system may be solved using a symbolic manipulator to obtain seven concrete expressions such as

$$f_0^{(0)} = \frac{\rho}{64}\left(-36+13|\mathbf{u}|^2-|\mathbf{u}|^4-\frac{12\gamma-62}{\gamma-1}\theta - \frac{5\gamma-3}{\gamma-1}\theta|\mathbf{u}|^2-\frac{2\gamma}{\gamma-1}\theta^2\right). \quad (41)$$

It is usually more computationally efficient to write equilibria like this, one formula for each value of i, rather than as one complicated expression involving weights w_i and the ξ_i that is valid for $i=-3,\ldots 3$. One typically gains efficiency from unrolling the resulting loop over i and precomputing the functions of ξ_i as constants.

8 One dimensional, split 4+3 velocity model

The poor stability properties of the early thermal lattice Boltzmann models led He *et al.* [13] to develop a split model using an entirely separate set of distribution functions to evolve the fluid's internal energy. They used a standard D2Q9 lattice for each distribution function, which meant that there were no particles with speed 2 or greater to cause instability, but also that their momentum equation contained artifacts due to the omission of the $\rho\mathbf{uuu}$ term in the third moment of the distribution function for density and momentum, our equation (21). This omission restricted the validity of their scheme to thermal flows at small Mach numbers, although they retained various terms such as viscous heating that would normally be neglected in a Boussinesq limit. As a side effect, use of two independent distribution functions, each with a BGK collision operator, enabled He *et al.* [13] to adjust the Prandtl number by varying the two relaxation times independently.

The mass and momentum conservation equations, including the Newtonian viscous stress, arise from equations (31) that do not involve the ϵ_i. One may therefore choose the $\boldsymbol{\xi}_i$ and $f_i^{(0)}$ to satisfy just the continuity and momentum equations, and obtain the complete energy equation from an entirely separate set of distribution functions g_i obeying a second discrete Boltzmann equation

$$\partial_t g_i + \boldsymbol{\zeta}_i\cdot\nabla g_i = -\frac{1}{\tau}(g_i - g_i^{(0)}), \quad (42)$$

with a possibly different set of discrete particle velocities $\boldsymbol{\zeta}_i$. The two discrete Boltzmann equations for f_i and g_i are coupled via the moments ρ, $\mathbf{u}$, and θ evaluated at lattice points. Achieving a realistic Prandtl number also requires coupling the equation for the g_i to the viscous stress computed from $f_i - f_i^{(0)}$.

The first few moments of the equilibria $g_i^{(0)}$ must be given by

$$\frac{1}{2}\sum_{i=0}^{N} g_i^{(0)} = \frac{\rho\,\theta}{\gamma-1}+\frac{1}{2}\rho|\mathbf{u}|^2, \quad (43a)$$

$$\frac{1}{2}\sum_{i=0}^{N} \boldsymbol{\zeta}_i g_i^{(0)} = \frac{\gamma}{\gamma-1}\rho\,\theta\,\mathbf{u}+\frac{1}{2}\rho|\mathbf{u}|^2\mathbf{u}, \quad (43b)$$

$$\frac{1}{2}\sum_{i=0}^{N} \boldsymbol{\zeta}_i\boldsymbol{\zeta}_i g_i^{(0)} = \frac{1}{2}\rho|\mathbf{u}|^2\mathbf{uu}+\frac{1}{2}\rho\theta|\mathbf{u}|^2\mathsf{I} + \frac{2\gamma-1}{\gamma-1}\rho\theta\mathbf{uu}+\frac{\gamma}{\gamma-1}\rho\theta^2\mathsf{I}. \quad (43c)$$

The left hand side of (43c) is a generic symmetric second rank tensor, unlike equation (36) before, so the $O(|\mathbf{u}|^2)$ terms need not be (and are not) the contraction of a symmetric fourth rank tensor.

Four momentum constraints in one dimension suggest using four particles with velocities $\xi_i=\{-2,-1,1,2\}$. In a departure from convention, there are no rest particles in this set of velocities. As before, the equilibria are given by the solution

$$\begin{aligned} f_{\pm2}^{(0)} &= \frac{1}{12}\rho\left(\pm u^3+2u^2\pm(3\theta-1)u+2\theta-2\right), \\ f_{\pm1}^{(0)} &= -\frac{1}{12}\rho\left(\pm 2u^3+2u^2\pm(6\theta-8)u+2\theta-8\right), \end{aligned} \quad (44)$$

to the four linear equations (31), rewritten in matrix form as

$$\begin{pmatrix} 1 & 1 & 1 & 1 \\ -2 & -1 & 1 & 2 \\ 4 & 1 & 1 & 4 \\ -8 & -1 & 1 & 8 \end{pmatrix} \begin{pmatrix} f_{-2}^{(0)} \\ f_{-1}^{(0)} \\ f_{1}^{(0)} \\ f_{2}^{(0)} \end{pmatrix} = \rho \begin{pmatrix} 1 \\ u \\ u^2+\theta \\ u^3+3\theta u \end{pmatrix}. \quad (45)$$

If one were to include an additional rest particle, there would be five equilibria to be found, but still only four constraint equations. This leaves one undetermined degree of freedom that may be adjusted to optimise stability [10].

The separate energy equation requires three constraints (43a-c), suggesting a separate set of three particle velocities $\zeta_i = \{-1, 0, 1\}$ that does include a rest particle to maintain symmetry. Writing the three constraint equations (43) in matrix form gives

$$\begin{pmatrix} 1 & 1 & 1 \\ -1 & 0 & 1 \\ 1 & 0 & 1 \end{pmatrix} \begin{pmatrix} g_{-1}^{(0)} \\ g_{0}^{(0)} \\ g_{1}^{(0)} \end{pmatrix} = \rho \begin{pmatrix} u^2 + 2\theta/(\gamma-1) \\ u^3 + 2\theta u\gamma/(\gamma-1) \\ u^4 + \theta u^2(5\gamma-3)/(\gamma-1) + 2\theta^2\gamma/(\gamma-1) \end{pmatrix} = \begin{pmatrix} S \\ V \\ T \end{pmatrix}. \quad (46)$$

The symbols S, V, T denote scalar, vector, and tensor quantities of the right hand side respectively (though only the x and xx components are present in this one-dimensional formulation). This particularly simple system has the solution

$$g_{-1}^{(0)} = \frac{1}{2}(T - V), \quad g_{0}^{(0)} = S - T, \quad g_{+1}^{(0)} = \frac{1}{2}(T + V). \quad (47)$$

9 Numerical implementation

The standard lattice Boltzmann method approximates the system of partial differential equations

$$\partial_t f_i + \boldsymbol{\xi}_i \cdot \nabla f_i = -\frac{1}{\tau}\left(f_i - f_i^{(0)}\right) \quad (48)$$

by the set of algebraic equations

$$\overline{f}_i(\mathbf{x} + \boldsymbol{\xi}_i \Delta t, t + \Delta t) - \overline{f}_i(\mathbf{x}, t) = -\frac{\Delta t}{\tau + \Delta t/2}\left(\overline{f}_i - f_i^{(0)}\right). \quad (49)$$

The $\overline{f}_i$ are related to the f_i by

$$\overline{f}_i = f_i + \frac{\Delta t}{2\tau}\left(f_i - f_i^{(0)}\right), \quad (50)$$

which renders (49) a second order accurate and fully explicit approximation to (1). Equation (49) may be derived by integrating (1) along characteristics for a time interval Δt using the trapezium rule [13]. However, although equation (49) is second order accurate for $\Delta t \ll \tau$, equation (49) causes the nonequilibrium part $\overline{f}_i - f_i^{(0)}$ to oscillate at every timestep when $\tau < \frac{1}{2}\Delta t$. By contrast, the original partial differential equation (1) always causes $f_i - f_i^{(0)}$ to decay monotonically towards zero on a timescale τ.

Moreover, when using particles with speeds 2 and larger, as needed to reproduce thermal behaviour, some information propagates 2 or more grid points per timestep under (49). Although the advective part of (49) is neutrally stable, consisting only of shifting data between grid points, it would not be surprising if the coupled system became unstable through violating the spirit of the Courant–Friedrichs–Lewy (CFL) stability condition – that information should propagate no further than one grid spacing per timestep.

This heuristic argument is not the whole story, because one isothermal D2Q13 scheme is stable enough to perform useful computations [38], and linearly stable D1Q5 schemes may be found for general barotropic equations of state [10]. However, Lallemand and Luo [18] found that the *thermal* D2Q13 scheme is linearly unstable due to an interaction between the energy flux and the shear stress. They proposed using a conventional finite difference method for the energy equation instead, but their finding of instability only applies to the standard space/time discretisation (49).

We therefore adopt an alternative space/time discretisation that does not suffer from either of these possible sources of instability. Using Strang splitting [33] we combine a solution of the advection equation $\partial_t f_i + \boldsymbol{\xi}_i \cdot \nabla f_i = 0$ from the Beam–Warming method [20, 37] with an exact solution of the collision equation. This splitting procedure resembles the "spin steps" used to implement the Coriolis force in a lattice Boltzmann ocean model [28]. The solution f_i^{new} to the discrete Boltzmann equation (1) after a timestep Δt is given by three steps, with intermediate values $f_i^\star$ and $f_i^{\star\star}$,

$$f_i^\star = f_i^{(0)} + (f_i - f_i^{(0)}) \exp\left(-\frac{1}{2}\frac{\Delta t}{\tau}\right), \quad (51a)$$

$$f_i^{\star\star}(x) = f_i^\star(x) - \frac{1}{2}|\xi_i|\frac{\Delta t}{\Delta x}\Big(3f_i^\star(x) - 4f_i^\star(x - \Delta x) + f_i^\star(x - 2\Delta x)\Big) + \frac{1}{2}\left(|\xi_i|\frac{\Delta t}{\Delta x}\right)^2\Big(f_i^\star(x) - 2f_i^\star(x - \Delta x) + f_i^\star(x - 2\Delta x)\Big), \quad (51b)$$

$$f_i^{(\text{new})} = f_i^{(0)} + (f_i^{\star\star} - f_i^{(0)}) \exp\left(-\frac{1}{2}\frac{\Delta t}{\tau}\right). \quad (51c)$$

The Beam–Warming formula (51b) is written for $\xi_i > 0$, and combines a second-order accurate upwind first difference for the advection with an upwind second difference for stability. For $\xi_i < 0$ one should replace $x - \Delta x$ by $x + \Delta x$, replace $x - 2\Delta x$ by $x + 2\Delta x$, and reverse the sign of the first term.

Since $f_i^{(0)}$ depends only on the quantities ρ, $\mathbf{u}$ and θ that are conserved under collisions, steps (51a) and (51c) give the exact solution to the system of ordinary differential equations

$$\partial_t f_i = -\frac{1}{\tau}(f_i - f_i^{(0)}) \tag{52}$$

over a time interval $\frac{1}{2}\Delta t$. In particular, these steps ensure that $f_i^{(\text{new})} \to f_i^{(0)}$ as $\tau \to 0$ even when $\Delta t \gg \tau$. This so-called asymptotic preserving property ensures that small τ values do not impose a stability constraint on the timestep Δt. However, there is an accuracy constraint due to the splitting of the coupled advection and collision equation (1) into three separate steps. The use of two collision steps (51a) and (51c), each for times $\frac{1}{2}\Delta t$, gives a splitting error of $O(\Delta t^2)$. The overall scheme thus has second-order accuracy in time. The two collision steps may be combined into one for an efficient implementation, except when the solution at a particular time $n\Delta t$ for integer n is required for output.

It is worth emphasising that the above split scheme leads to accurate results when $\Delta t \approx \tau$, with little benefit from taking $\Delta t \ll \tau$, but the splitting error leads to overly diffusive behaviour when $\Delta t \gg \tau$. Unlike the standard lattice Boltzmann scheme (49), the split scheme does not capture the correct behaviour of slowly varying solutions of the discrete Boltzmann PDE (48) when $\Delta t \gg \tau$. This limitation is shared by other approximations to the discrete Boltzmann PDE, such as finite volume approximations to the isothermal discrete Boltzmann PDE on unstructured meshes [36]. It is perhaps a less severe restriction for simulations of compressible flow with shocks, since substantially more dissipation is required to resolve shocks than is required to resolve shear layers in incompressible flows. The thickness of shocks is proportional to the viscosity μ, while the thickness of shear layers is proportional to $\mu^{1/2}$. In other words, the resolution of shocks in a compressible flow requires a grid-scale Reynolds number of order unity, in the absence of some kind of solution-adaptive dissipation.

10 Changing the Prandtl number

Using the unsplit approach of Sec. 7 with the BGK collision operator leads to non-equilibrium momentum and energy fluxes given by

$$\begin{aligned} \boldsymbol{\Pi}^{(1)} &= -\mu\left[(\nabla\mathbf{u}) + (\nabla\mathbf{u})^{\mathsf{T}} - (\gamma-1)\mathsf{I}\nabla\cdot\mathbf{u}\right], \\ \boldsymbol{\mathcal{F}}^{(1)} &= \mathbf{u}\cdot\boldsymbol{\Pi}^{(1)} - \kappa\nabla\theta, \end{aligned} \tag{53}$$

with viscosity $\mu = \tau\rho\theta$ and thermal conductivity $\kappa = \mu\gamma/(\gamma-1)$. This corresponds to a Prandtl number $\mathrm{Pr} = (\nu/\kappa)\cdot(\gamma-1)/\gamma$ of unity in standard kinetic theory usage, but the true value of the Prandtl number should be close to 2/3, and exactly 2/3 for a gas of Maxwell molecules.

To adjust the value of κ independently of the μ appearing inside $\boldsymbol{\Pi}^{(1)}$ in the second of equations (53), thus leaving the viscous heating correct, it is necessary to adopt a collision operator that is non-diagonal in the basis of moments with respect to the particle velocity $\boldsymbol{\xi}_i$. In continuum kinetic theory there is no difficulty because it is standard to use moments with respect to the so-called peculiar velocity $\mathbf{c} = \boldsymbol{\xi}_i - \mathbf{u}$ instead. This separates the $\mathbf{u}\cdot\boldsymbol{\Pi}^{(1)}$ and $-\kappa\nabla\theta$ contributions of the energy flux, so one may use various extensions of the BGK collision operator such as the Gross–Jackson [11] or Shakhov S-model [29] that allow arbitrary Prandtl number, yet are diagonal in a basis of moments with respect to the peculiar velocity. Transforming back to a basis of moment with respect to $\boldsymbol{\xi}_i$ yields a non-diagonal collision operator, but one that can still be solved exactly using exponentials. Further investigation, and a detailed study of the splitting method, will presented elsewhere.

In addition, a constant value for the collision time τ, adopted here for simplicity, gives a dynamic viscosity $\mu = \tau\rho\theta$ that is proportional to the product of density and temperature. This is an artifact of the BGK collision operator. The viscosity in a dilute monatomic gas is proportional to $\theta^{1/2}$ and independent of density. At fixed temperature, the longer mean free path in a lower density gas precisely compensating for the smaller number of atoms per unit volume transporting momentum. The temperature dependence for diatomic gases is commonly modelled by Sutherland's law,

$$\mu = \mu_{\text{ref}}\left(\frac{\theta}{\theta_{\text{ref}}}\right)^{3/2}\frac{\theta_{\text{ref}}+\theta_{\text{S}}}{\theta+\theta_{\text{S}}}. \tag{54}$$

Here μ_{ref} is the viscosity at a reference temperature θ_{ref}, and θ_{S} is a constant (equivalent to 111 Kelvin for air). Sutherland's law asymptotes to the monatomic gas behaviour at high temperatures, $\mu \sim \theta^{1/2}$ when $\theta \gg \theta_{\text{S}}$. A more accurate simulation would take the energy and momentum relaxation times to be separate functions of the density and temperature at lattice points, chosen to give the desired functional dependence of the viscosity and thermal conductivity on temperature (as in [21]).

11 Numerical results

Figure 1 shows the results of simulating Sod's first shock tube problem [20, 32] using the unsplit seven velocity model of Sec. 7 with $\gamma = 5/3$. The initial conditions for this benchmark problem correspond to a stationary gas with density and pressure given by

$$\begin{aligned} \rho = 1.0 \text{ and} \quad & p = 1.0 \text{ for } x < 0, \\ \rho = 0.125 \text{ and} \quad & p = 0.1 \text{ for } x > 0. \end{aligned} \tag{55}$$

The computation was performed on the domain $-0.5 \le x < 0.5$ using 4096 points and periodic boundary conditions. There is thus a second backwards-facing shock tube at the periodic boundary, but the two Riemann fans have not had time to interact by the time $t = 0.1$ shown in the figure. The computations used a BGK collision operator

with $\tau = 10^{-4}$, and a timestep Δt set by the maximum Courant number $3\Delta t/\Delta x = 0.9$. For these parameter values the ratio $\Delta t/\tau \approx 0.8$ is not especially small, but the solution was left virtually unchanged by taking much smaller timesteps.

The solution computed with fixed τ is in close agreement with a reference solution of the compressible Euler equations computed using the second order accurate extension by Kurganov and Tadmor [17] of the local Lax–Friedrichs (or Rusanov) scheme. The system of ordinary differential equations arising from this semi-discrete scheme was solved using a second order, total variation diminishing, Runge–Kutta integrator [31]. The discrete Boltzmann solution shows a small velocity overshoot due to insufficient dissipation at the shock, and a velocity perturbation near the contact discontinuity.

Total variation diminishing (TVD) methods for computational gas dynamics capture shocks without overshoots, and without excessive global dissipation, by increasing the dissipation in the neighbourhood of large spatial gradients (see *e.g.* Laney [20]). The so-called entropic lattice Boltzmann methods achieve a similar goal by adjusting the relaxation time depending upon the non-equilibrium part of the distribution functions, which in turn depends upon local spatial gradients (see *e.g.* Boghosian *et al.* [4]). A fully competitive Boltzmann scheme for polyatomic gases is likely to require the implementation of an entropic approach to improve shock capturing in comparison with computations using a uniform relaxation time as presented here.

Figure 2 compares the non-equilibrium momentum and energy fluxes $\Pi_{xx} - \Pi_{xx}^{(0)}$ and $\mathcal{F}_x - \mathcal{F}_x^{(0)}$ with their Navier–Stokes–Fourier values,

$$\begin{aligned} \Pi_{xx}^{\mathrm{NSF}} - \Pi_{xx}^{(0)} &= -(4/3)\tau\rho\theta u_x, \\ \mathcal{F}_x^{\mathrm{NSF}} - \mathcal{F}_x^{(0)} &= -(4/3)\tau\rho\theta u u_x - (5/2)\tau\rho\theta\theta_x, \end{aligned} \tag{56}$$

as computed from the numerical values of ρ, u, and θ, and second order centred differences for their derivatives. The actual non-equilibrium fluxes are in close agreement with their Navier–Stokes–Fourier values, except in the region of the contact discontinuity where $\Pi_{xx} - \Pi_{xx}^{(0)}$ has the wrong sign compared with the Navier–Stokes viscous stress. The true solution should have spatially uniform velocity at the contact discontinuity, which is marked by a jump in density only, so the Navier–Stokes viscous stress should vanish. The discrepancy may be due to finite Knudsen number (finite τ) effects, or a consequence of initialising with the piecewise constant initial data (55).

Figures 3 and 4 show the corresponding data for a diatomic gas with $\gamma = 7/5$. The previous initial conditions were scaled by a factor of 1/4 in the pressure to achieve a stable computation,

$$\begin{aligned} \rho = 1.0 \text{ and } \quad p = 0.25 \text{ for } x < 0, \\ \rho = 0.125 \text{ and } \quad p = 0.025 \text{ for } x > 0. \end{aligned} \tag{57}$$

There is no fixed relation between the temperature and the particle velocities in discrete kinetic theory, since the dis-

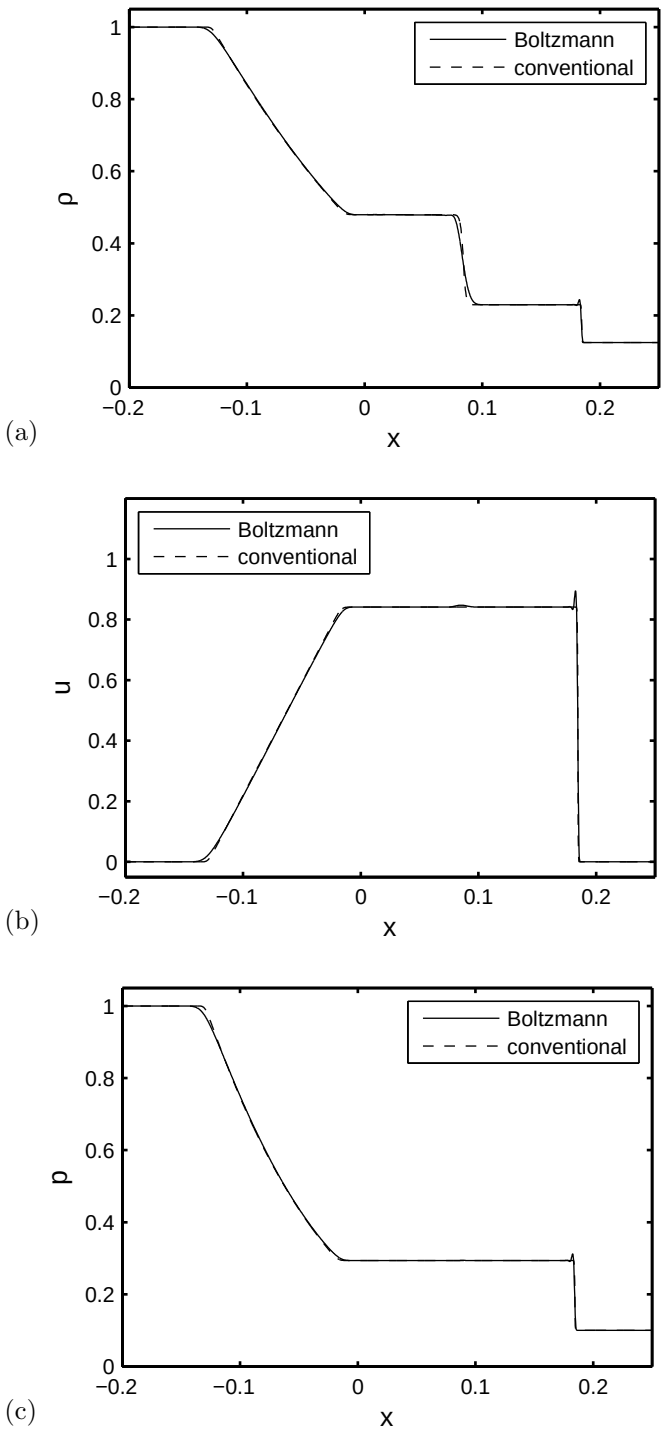

Figure 1: Comparison of (a) the density, (b) the velocity, and (c) the pressure for Sod's first shock tube problem with $\gamma = 5/3$ at time $t = 0.1$. Results from the unsplit Boltzmann scheme are shown solid, and a conventional numerical solution for the inviscid problem is shown dotted. There is a small velocity overshoot at the shock, and a bump at the contact discontinuity near $x = 0.07$.

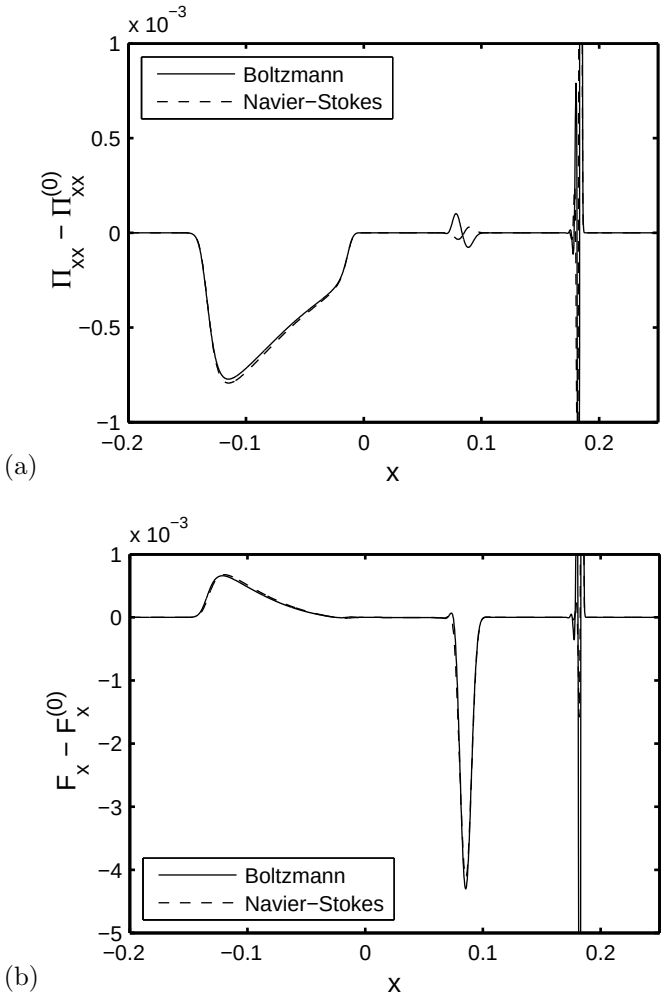

Figure 2: Comparison of (a) the viscous stress, and (b) the diffusive energy flux, for the same computation as Fig. 1. The non-equilibrium parts of Π_{xx} and $\mathcal{F}_x$ are shown solid, and the Navier–Stokes–Fourier values for these quantities obtained from the computed values of ρ, u, θ are shown dotted. There is good agreement apart from the viscous stress near the contact discontinuity, where the true solution should have spatially uniform velocity.

crete equilibria $f_i^{(0)}$ are not constrained by the functional form of the continuum Maxwell–Boltzmann distribution involving the ratio $|\boldsymbol{\xi} - \mathbf{u}|^2/\theta$. Conversely, it is reasonable to expect that some relation between the square root of temperature, or isothermal sound speed, and the particle velocities will be necessary for stability. For instance, stability would be highly unlikely if the sound speed exceeded the fastest particle speed. One may recover the solution of the original unscaled problem by suitably scaling the fluid velocity, timescale, and transport coefficients in the simulation.

Again, there is reasonable agreement between the discrete Boltzmann solution, performed on a grid of 8192 points with $\tau = 10^{-4}$ as before, and the reference solution of the inviscid equations. A perturbation in velocity near the contact discontinuity is no longer noticeable, compare Fig. 1(b) with Fig. 3(b), but discrepancies in the non-equilibrium fluxes near the contact discontinuity are noticeably larger. The latter may be partly because the magnitudes of the Navier–Stokes–Fourier viscous stress and energy flux are roughly a factor of 8 smaller due to the rescaling of temperature and velocity in (57).

The split 4+3 velocity model developed in Sec. 8 turns out to be much less stable than the unsplit 7 velocity model. Figure 5 shows a comparison of the density computed using both the split 4+3 velocity and unsplit 7 velocity models. However, even with $\gamma = 5/3$ and the rescaled temperature, it was necessary to smooth out the initial data using a tanh function so that the initial gradient was no more than 50 in modulus. Both computations used a grid with 4096 points, $\tau = 10^{-4}$, and maximum Courant number of 0.9. However, the split model uses 50% longer timesteps because the maximum particle speed is 2, rather than 3, in the CFL stability criterion.

12 Conclusion

We have derived a set of moment equations leading to the compressible Navier–Stokes–Fourier equations with arbitrary adiabatic exponent γ, and a correct, Galilean-invariant viscous stress and energy flux. For general γ the usual monatomic gas relations $\mathcal{E} = \frac{1}{2}\mathrm{Tr}\,\boldsymbol{\Pi}$ and $\boldsymbol{\mathcal{F}} = \frac{1}{2}\mathrm{Tr}\,(\sum_i \boldsymbol{\xi}_i\boldsymbol{\xi}_i\boldsymbol{\xi}_i f_i)$ do not hold, so it is necessary to introduce additional degrees of freedom to satisfy the constraints on $\mathcal{E}$ and $\boldsymbol{\mathcal{F}}$ independently of those for the momentum flux $\boldsymbol{\Pi}$ and complete third moment $\sum_i \boldsymbol{\xi}_i\boldsymbol{\xi}_i\boldsymbol{\xi}_i f_i$.

One may either assign additional internal energies to particles, allowing the moments of f_i in the energy equation to be adjusted independently of those in the momentum equation, or introduce a completely separate set of distribution functions g_i for just the energy equation. In either case, there are seven moment constraints in one spatial dimension, requiring at least seven different particle velocities to satisfy them. By contrast, five particle velocities are sufficient to reproduce the Navier–Stokes–Fourier equations with the natural $\gamma = 3$ for one-dimensional kinetic theory [9]. The unsplit 7 velocity model developed in Sec. 7 stably simulates the first Sod shock tube problem for both $\gamma = 5/3$ (monatomic) and $\gamma = 7/5$ (diatomic). The split 4+3 velocity model is noticeably less stable, but allows the use of longer timesteps. However, the space/time discretisation in Sec. 9 using Strang splitting and Beam–Warming advection is just one of many possible numerical implementations.

In discrete kinetic theory there is no fixed relation between the sound speed, as given by the temperature, and the particle speeds. The temperature θ is a free parameter in all the discrete equilibrium distributions given in this paper. The fluid velocity and the sound speed may thus both be rescaled with respect to the particle speeds without changing the Mach number, the ratio of the fluid velocity to the sound speed. The finite particle speeds thus

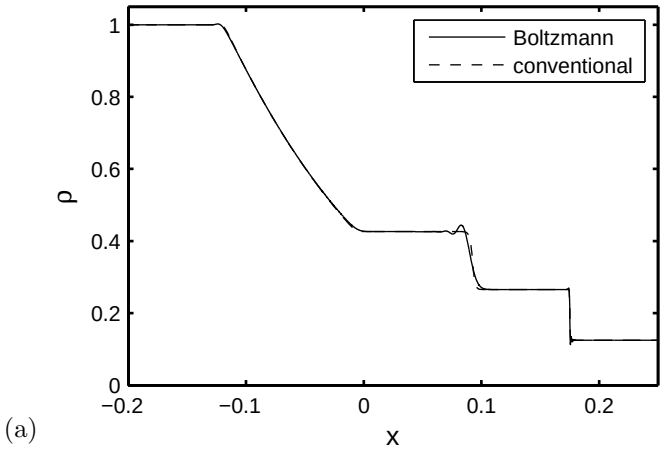

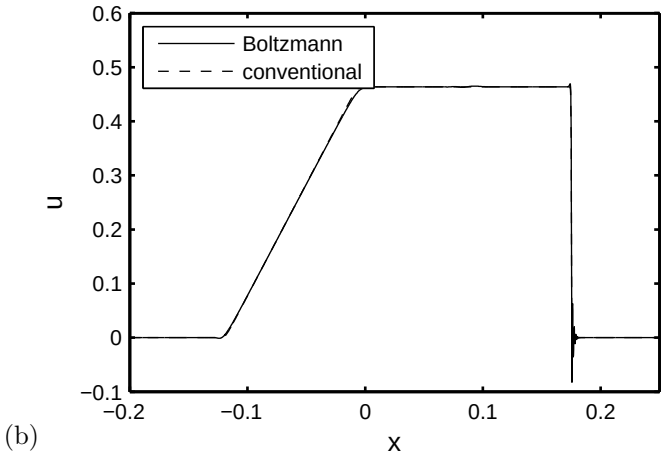

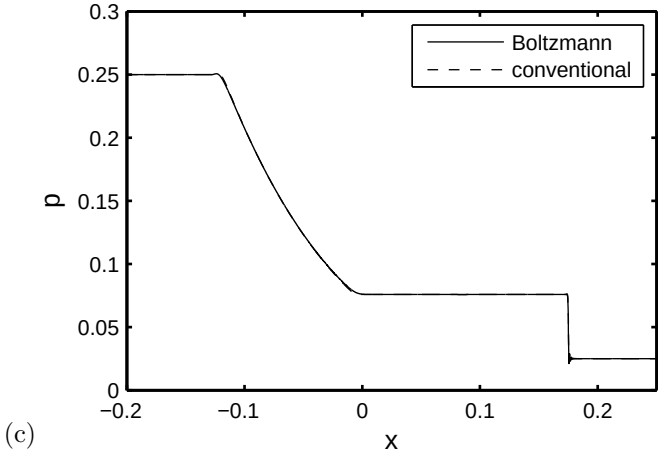

Figure 3: Comparison of (a) the density, (b) the velocity, and (c) the pressure for Sod's first shock tube problem with $\gamma = 7/5$ at time $t = 0.2$. The pressure and temperature have been scaled by a factor of $1/4$ to bring them inside the stability window of the discrete Boltzmann scheme, which has the effect of halving the velocity. Results from the unsplit Boltzmann scheme are shown solid, and a conventional numerical solution of the inviscid problem is shown dotted.

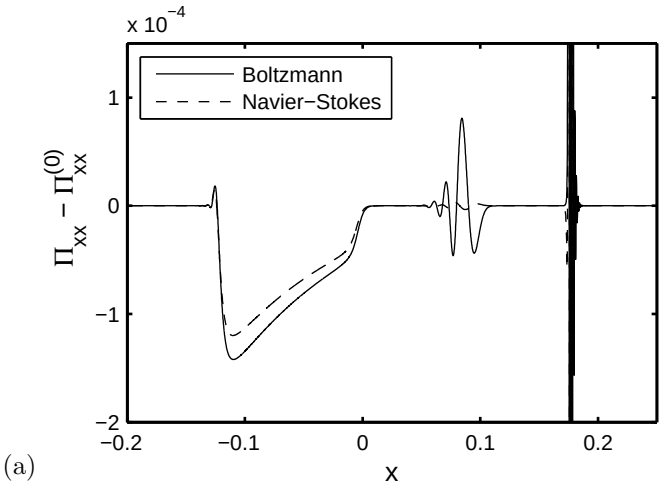

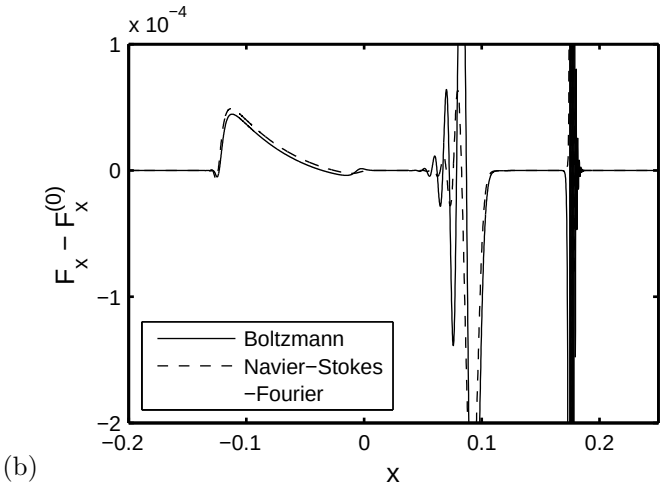

Figure 4: Comparison of (a) the viscous stress, and (b) the diffusive energy flux, for the same problem. The non-equilibrium parts of Π_{xx} and $\mathcal{F}_x$ are shown solid, and the Navier–Stokes–Fourier values for these quantities computed from the numerical values of ρ, u, θ are shown dotted. There is reasonable agreement except near the contact discontinuity ($x \approx 0.08$), where the true solution should have spatially uniform velocity.

place no restriction on the flows that may be simulated.

When extending to two or more spatial dimensions, the number of degrees of freedom needed to satisfy the moment constraints is typically few than the number needed for isotropy. For example, in two dimensions the split model requires 10 degrees of freedom for the momentum equation, with distribution functions f_i, and another 6 for the energy equation with distribution functions g_i. Existing lattice Boltzmann models [21, 38] using the so-called D2Q13 square lattice could be adapted to simulate the density and momentum equations in the split model. The second discrete Boltzmann equation for the g_i could be implemented on the common D2Q9 lattice, as in the Boussinesq-like thermal lattice Boltzmann model of He *et al.* [13]. This leaves 6 degrees of freedom that could in principle be cho-

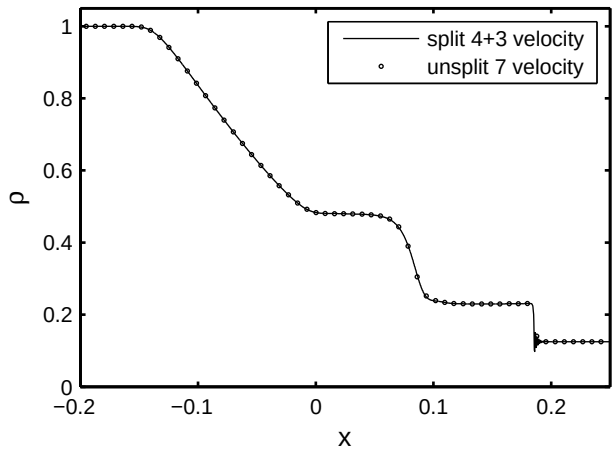

Figure 5: Comparison of density between the split 4+3 velocity and unsplit 7 velocity models for the same initial conditions corresponding to a smoothed out Sod shock tube with rescaled temperature, as in equation (57).

sen arbitrarily, but may be tuned to optimise stability [10].

REFERENCES

[1] Alexander, F., Chen, S., and Sterling, J. (1993). Lattice Boltzmann thermohydrodynamics. *Phys. Rev. E*, 47:R2249–R2252.

[2] Ansumali, S., Karlin, I. V., Frouzakis, C. E., and Boulouchos, K. B. (2006). Entropic lattice Boltzmann method for microflows. *Physica A*, 359:289–305.

[3] Bhatnagar, P. L., Gross, E. P., and Krook, M. (1954). A model for collision processes in gases. I. Small amplitude processes in charged and neutral one-component system. *Phys. Rev.*, 94:511–525.

[4] Boghosian, B. M., Yepez, J., Coveney, P. V., and Wagner, A. (2001). Entropic lattice Boltzmann methods. *Proc. R. Soc. Lond. A*, 457:717–766.

[5] Chen, Y., Ohashi, H., and Akiyama, M. (1994). Thermal lattice Bhatnagar–Gross–Krook model without nonlinear deviations in macrodynamic equations. *Phys. Rev. E*, 50:2776–2783.

[6] Dellar, P. J. (2001). Bulk and shear viscosities in lattice Boltzmann equations. *Phys. Rev. E*, 64:031203.

[7] Dellar, P. J. (2002a). Compound waves in a thermohydrodynamic lattice BGK scheme using non-perturbative equilibria. *Europhys. Lett.*, 57:690–696.

[8] Dellar, P. J. (2002b). Lattice kinetic schemes for magnetohydrodynamics. *J. Comput. Phys.*, 179:95–126.

[9] Dellar, P. J. (2005). Lattice and discrete Boltzmann equations for fully compressible flow. In Bathe, K.-J., editor, *Computational Fluid and Solid Mechanics*, pages 632–635, Amsterdam. Proceedings of The Third MIT Conference on Computational Fluid and Solid Mechanics, Elsevier.

[10] Dellar, P. J. (2006). Non-hydrodynamic modes and general equations of state in lattice Boltzmann equations. *Physica A*, 362:132–138.

[11] Gross, E. P. and Jackson, E. A. (1959). Kinetic models and the linearized Boltzmann equation. *Phys. Fluids*, 2:432–441.

[12] Hanson, F. B. and Morse, T. F. (1967). Kinetic models for a gas with internal structure. *Phys. Fluids*, 10:345–353.

[13] He, X., Chen, S., and Doolen, G. D. (1998). A novel thermal model of the lattice Boltzmann method in incompressible limit. *J. Comput. Phys.*, 146:282–300.

[14] Kataoka, T. and Tsutahara, M. (2004). Lattice Boltzmann model for the compressible Navier–Stokes equations with flexible specific-heat ratio. *Phys. Rev. E*, 69:035701–4.

[15] Kogan, A. M. (1965). Derivation of Grad's type equations and study of their relaxation properties by the method of maximization of entropy. *J. Appl. Math. Mech.*, 29:130–142.

[16] Kogan, M. N. (1973). Molecular gas dynamics. *Annu. Rev. Fluid Mech.*, 5:383–404.

[17] Kurganov, A. and Tadmor, E. (2000). New high-resolution central schemes for nonlinear conservation laws and convection-diffusion equations. *J. Comput. Phys.*, 160:241–282.

[18] Lallemand, P. and Luo, L.-S. (2003). Hybrid finite-difference thermal lattice Boltzmann equation. *Int. J. Mod. Phys. B*, 17:41–48.

[19] Landau, L. D. and Lifshitz, E. M. (1987). *Fluid Mechanics*. Pergamon, Oxford, 2nd edition.

[20] Laney, C. B. (1998). *Computational Gasdynamics*. Cambridge University Press, Cambridge.

[21] Li, X. M., Leung, R. C. K., and So, R. M. C. (2006). One-step aeroacoustics simulation using lattice Boltzmann method. *AIAA J.*, 44:78–89.

[22] McNamara, G. R., Garcia, A. L., and Alder, B. J. (1995). Stabilization of thermal lattice Boltzmann models. *J. Statist. Phys.*, 81:395–408.

[23] Morse, T. F. (1964). Kinetic model for gases with internal degrees of freedom. *Phys. Fluids*, 7:159–169.

[24] Quirk, J. J. (1994). A contribution to the great Riemann solver debate. *Int. J. Numer. Meth. Fluids*, 18:555–574.

[25] Reider, M. and Sterling, J. (1995). Accuracy of discrete-velocity BGK models for the simulation of the incompressible Navier–Stokes equations. *Comput. & Fluids*, 24:459–467.

[26] Renda, A., Bella, G., Succi, S., and Karlin, I. V. (1998). Thermohydrodynamic lattice BGK schemes with non-perturbative equilibria. *Europhys. Lett.*, 41:279–283.

[27] Roe, P. L. (1981). Approximate Riemann solvers, parameter vectors, and difference schemes. *J. Comput. Phys.*, 43:357–372.

[28] Salmon, R. (1999). Lattice Boltzmann solutions of the three-dimensional planetary geostrophic equations. *J. Marine Res.*, 57:847–884.

[29] Shakhov, E. M. (1968). Generalization of the Krook kinetic relaxation equation. *Fluid Dynamics*, 3:95–96.

[30] Shi, W., Shyy, W., and Mei, R. (2001). Finite-difference-based lattice Boltzmann method for inviscid compressible flows. *Numer. Heat Transfer B*, 40:1–21.

[31] Shu, C.-W. and Osher, S. (1989). Efficient implementation of essentially non-oscillatory shock-capturing schemes, II. *J. Comput. Phys.*, 83:32–78.

[32] Sod, G. A. (1978). A survey of several finite difference methods for systems of nonlinear hyperbolic conservation laws. *J. Comput. Phys.*, 27:1–31.

[33] Strang, G. (1968). On the construction and comparison of difference schemes. *SIAM J. Numer. Anal.*, 5:506–517.

[34] Taxman, N. (1958). Classical theory of transport phenomena in dilute polyatomic gases. *Phys. Rev.*, 110:1235–1239.

[35] Toschi, F. and Succi, S. (2005). Lattice Boltzmann method at finite Knudsen numbers. *Europhys. Lett.*, 69:549–555.

[36] Ubertini, S. and Succi, S. (2005). Recent advances of lattice Boltzmann techniques on unstructured grids. *Prog. Comput. Fluid Dynam.*, 5:85–96.

[37] Warming, R. F. and Beam, R. M. (1976). Upwind second-order difference schemes and applications in aerodynamic flows. *AIAA J.*, 14:1241–1249.

[38] Weimar, J. R. and Boon, J. P. (1996). Nonlinear reactions advected by a flow. *Physica A*, 224:207–215.

[39] Xu, K. (2001). A gas-kinetic BGK scheme for the Navier–Stokes equations and its connection with artificial dissipation and Godunov method. *J. Comput. Phys.*, 171:289–335.

[40] Zhang, Y., Qin, R., and Emerson, D. R. (2005). Lattice Boltzmann simulation of rarefied gas flows in microchannels. *Phys. Rev. E*, 71:047702–4.